SCIENCE CHINA
Information Sciences

• RESEARCH PAPER •

June 2016, Vol. 59 062309:1–062309:13
doi: 10.1007/s11432-015-5480-x

Novel estimators of equivalent number of looks in polarimetric SAR imagery based on sub-matrices

Tao LIU[1]*, Haogui CUI[2], Zemin XI[1] & Jun GAO[1]

[1]*School of Electronic Engineering, Naval University of Engineering, Wuhan* 430033*, China;*
[2]*Marine Communication Technology Institute, Beijing* 100841*, China*

Received July 30, 2015; accepted September 14, 2015; published online April 18, 2016

Abstract The equivalent number of looks (ENL) is an important parameter in the multilook statistical model of polarimetric synthetic aperture radar (Pol-SAR). Recently, the maximum likelihood (ML) method was proposed and gave a good performance in the Gaussian model case by using the full covariance matrix instead of the intensity of Pol-SAR data, but it generated underestimates in the product model case. In this paper several novel ENL estimators are presented via certain cumulants of the log-determinant of the sub-matrices of the multilook polarimetric covariance matrix. The texture effect to the ENL estimates is eliminated, and the analytic estimators are derived. The estimators use the full covariance matrix and sub-matrices information, rather than the intensities of polarization channels. All the novel estimators are suitable for any texture model and thus provide more accurate results than many existing ones. Experiments using simulated data and real data are presented to evaluate the performance of different estimators. The results show that the second log-determinant moment (SLDM3)-based method is the best one among the novel estimators. At the same time this estimator has much less computational complexity. In addition, a novel distribution classification method is proposed by coloring the image via second- and third-order log-cumulants of the covariance matrix (MLC), which is helpful to assess the estimation result.

Keywords radar polarimetry, synthetic aperture radar, parameter estimation, moment methods, sub-matrix, log-cumulants

Citation Liu T, Cui H G, Xi Z M, et al. Novel estimators of equivalent number of looks in polarimetric SAR imagery based on sub-matrices. Sci China Inf Sci, 2016, 59(6): 062309, doi: 10.1007/s11432-015-5480-x

1 Introduction

The equivalent number of looks (ENL) describes the degree of averaging during data formation and post-processing in multilook synthetic aperture radar (SAR) images [1]. Speckle is a characteristic of all coherent imaging systems. Multilooking can suppress the effect of it. The correlated measurements are averaged by multilooking, while the correlation makes the number of looks not suitable for a real data model [1]. To solve this problem, we can replace the actual number of correlated samples by an equivalent number of independent ones [1]. The ENL is the parameter value that leads to a best match between theoretical moments of the independent data model and empirical moments of the correlated data. Multilooking processing is normally performed in the frequency domain. Multiple measurements

* Corresponding author (email: liutao1018@sina.com)

are derived by dividing the synthetic aperture Doppler bandwidth into several sub-bands, as looks from different sight angles [2,3]. Multilook data are derived by averaging the nearby pixels in the spatial domain. At the same time, multilooking can also be performed as post-processing after the image has formed. Both approaches to multilooking suppress the speckle and reduce image resolution, and therefore they can ease the computational burden of SAR imagery data [1].

The ENL, as a distribution parameter, influences the information accuracy extracted by methods based upon the statistical modeling of multilook SAR data [4–9]. The ENL is commonly estimated by selecting homogeneous regions in an image, where the speckle is fully developed. That is to say that the scattering coefficients are assumed to be complex Gaussian distributed or that the covariance matrix obeys a Wishart distribution [2]. The ENL can be estimated from these image statistical characteristics. But the required identification of homogeneous regions makes these methods difficult to design and apply in reality. In the area of inhomogeneity, underestimation of the ENL will occur generally [1].

The conventional ENL estimators have been presented for the case of single-polarization SAR [2,3]. For PolSAR data, the ENL has traditionally been estimated separately for each polarimetric channel, and then averaged, as shown in [7,10]. Anfinsen et al. [1] developed a general analytical theory for fully polarimetric SAR data, in which the polarization information in the Gaussian data model was fully used (trace moment-based estimator, TME; maximum likelihood estimator, MLE) . We developed the TME method as DTM, which is suitable for product model, while this method is only suitable for same speckle statistics cases (similar scattering mechanism) [11]. Doulgeris et al. [12] then proposed a texture-corrected ENL estimator with the log-cumulants method. This texture-corrected method estimates the texture parameters of the K-Wishart model firstly, and the ENL estimation is the numerical solution from the first-order log-cumulant (FOL) expression. But this method costs much time and can be applied only to K distribution. Sometimes it will be invalid due to its incorrect estimation of the shape parameters. Therefore, it is of great importance to find a novel method to estimate the ENL accurately, and which is robust for both the Gaussian model and the product model. The objective of this work is to establish a theory of ENL estimation for the polarimetric case, where estimates are derived explicitly from matrix-variate statistics in both the Gaussian and the product models.

The paper is structured as follows. Section 2 reviews the literature of known estimators for polarimetric case, showing that they are limited to the product model case, and we present the novel ENL estimators based on sub-matrices of the covariance matrix, which are adaptive to both the Gaussian model case and the product model case. Section 3 presents the experimental results with synthetic data and real data. In Section 4 we give the conclusion.

2 Novel estimators

The existing estimators, such as trace moment-based (TM) estimator [1], the developed TM (DTM) estimator [11], log-determinant moment-based estimator (ML) [1], and first-order log-cumulants estimator (FOL) [12], using a full polarimetric matrix, is better than using only one single polarization channel. In MLE case, when the sample size is small, the estimates can be corrected by estimating $|\boldsymbol{\Sigma}|$ using MLE [13]. This can be named the ML-ML estimator. It can be concluded that all the existing estimators are not suitable for the product model case, and this is the motivation for our work. We have therefore tried to derive a log-cumulants based estimator which can be effectively adapted to both the Gaussian case and the product model case via the full information used in the determinants of the sub-matrices of different order with 1×1, 2×2, and 3×3.

We have therefore tried to derive a log-cumulants based estimator which can be effectively adapted to both the Gaussian case and the product model case via the full information used in the determinants of the sub-matrices of different order with different dimensions as 1×1, 2×2, and 3×3.

Assume that the random covariance matrix $\boldsymbol{Z} = L\boldsymbol{C}$ with L the number of looks is the covariance matrix of multi-look imagery and may belong to the product model case and the scale matrix $\boldsymbol{\Sigma} = \mathrm{E}\{\boldsymbol{Z}\}/L = \mathrm{E}\{\boldsymbol{C}\}$, where E{} is the expectation operator. For a clear demonstration, the matrix log-

cumulants (MLCs) of $\boldsymbol{C}$ evaluate under the product model to [14]:

$$\tilde{k}_{1,d}\{\boldsymbol{C}_d\} = \psi_d^{(0)}(L) + \ln|\boldsymbol{\Sigma}_d| - d(\ln L - \tilde{k}_1\{T\}), \tag{1}$$

where $|\cdot|$ is the determinant operator, the subscript 1 represents the first order of the log-cumulants, d is the dimension of the sub-matrix, $\tilde{k}_1\{\}$ means the first order log-cumulants, $\Gamma(L)$ is the gamma function, $\psi^{(0)}(L) = \Gamma'(L)/\Gamma(L)$ is known as the digamma function, defined as

$$\psi^{(m)}(z) = \frac{d^{m+1}}{dL^{m+1}}\ln\Gamma(L) = (-1)^m\int_0^\infty \frac{t^m \mathrm{e}^{-zt}}{1-\mathrm{e}^{-t}}\mathrm{d}t, \tag{2}$$

and $\psi_d^{(0)}(L) = \sum_{i=0}^{d-1}\psi^{(0)}(L-i)$. The sum of polygamma functions satisfies the following relation:

$$\psi^{(m)}(z+1) - \psi^{(m)}(z) = (-1)^m m! z^{-(m+1)}. \tag{3}$$

2.1 Second log-determinant moment-based estimator (SLDM)

In order to eliminate the effect of the textural variable, we use the log-determinant of the one and two dimensions covariance matrices in Eq. (1).

If $d = 1$, we get

$$\tilde{k}_{1,1}\{\boldsymbol{C}_1\} = \psi^{(0)}(L) + \ln|\boldsymbol{\Sigma}_1| - (\ln L - \tilde{k}_1\{T\}). \tag{4}$$

If $d = 2$, we get

$$\tilde{k}_{1,2}\{\boldsymbol{C}_2\} = \psi^{(0)}(L) + \psi^{(0)}(L-1) + \ln|\boldsymbol{\Sigma}_2| - 2(\ln L - \tilde{k}_1\{T\}). \tag{5}$$

If $d = 3$, we get

$$\tilde{k}_{1,3}\{\boldsymbol{C}_3\} = \psi^{(0)}(L) + \psi^{(0)}(L-1) + \psi^{(0)}(L-2) + \ln|\boldsymbol{\Sigma}_3| - 3(\ln L - \tilde{k}_1\{T\}). \tag{6}$$

Eq. (4) $\times$ 2$-$Eq. (5), using Eq. (3), we get

$$L = 1 + \frac{1}{(2\tilde{k}_{1,1}\{\boldsymbol{C}_1\} - \tilde{k}_{1,2}\{\boldsymbol{C}_2\}) - (2\ln|\boldsymbol{\Sigma}_1| - \ln|\boldsymbol{\Sigma}_2|)}. \tag{7}$$

Here the texture variable has been eliminated. The log-cumulant of the first order of $\boldsymbol{C}_1$ can be obtained from three elements of $\boldsymbol{C}_{11}, \boldsymbol{C}_{22}$ and $\boldsymbol{C}_{33}$ and so is the log-cumulant of the first order of $\boldsymbol{C}_2$ from the sub-matrix with 2$\times$2 elements. The estimator is as follows:

$$\hat{L}_{\mathrm{SLDM}} = 1 + \frac{1}{(2\langle\ln\boldsymbol{C}_1\rangle - \langle\ln\boldsymbol{C}_2\rangle) - (2\ln|\langle\boldsymbol{C}_1\rangle| - \ln|\langle\boldsymbol{C}_2\rangle|)}. \tag{8.1}$$

The experimental results are given in Section 3. The performance is close to that of the ML, and the estimator can be directly applied to the product model case, with $\hat{L}_{\mathrm{SLDM}} \geqslant 2$. But in this estimator the determinant of the 3$\times$3 matrix has not been used. Therefore we give the next estimator.

In another way, we can resolve the solution of the estimation from $d = 2$ and $d = 3$ in Eq. (1). The estimation of the second and third SLDM method is using Eq. (5) $\times$ 3 $-$ Eq. (6) $\times$ 2, then we can get

$$\begin{cases} \hat{L}_{\mathrm{SLDM2}} = \dfrac{3(\hat{K}+1) + \sqrt{(\hat{K}+1)^2+8}}{2\hat{K}}, \\ \hat{K} = (3\langle\ln|\boldsymbol{C}_2|\rangle - 2\langle\ln|\boldsymbol{C}_3|\rangle) - (3\ln|\langle\boldsymbol{C}_2\rangle| - 2\ln|\langle\boldsymbol{C}_3\rangle|). \end{cases} \tag{8.2}$$

Using the same method as (Eq. (4) $\times$ 3 $-$ Eq. (6)), we can get

$$\begin{cases} \hat{L}_{\mathrm{SLDM3}} = \dfrac{3(\hat{K}+1) + \sqrt{(\hat{K}-1)^2+8}}{2\hat{K}}, \\ \hat{K} = (3\langle\ln|\boldsymbol{C}_1|\rangle - \langle\ln|\boldsymbol{C}_3|\rangle) - (3\ln|\langle\boldsymbol{C}_1\rangle| - \ln|\langle\boldsymbol{C}_3\rangle|). \end{cases} \tag{8.3}$$

All of the SLDM methods do not use the full information of the covariance matrix log-determinant cumulants, and the following will give the methods that use the full information.

2.2 Third log-determinant moment-based estimator (TLDM)

We can obtain the equation as follows from Eq. (1) when $d = 1, 2, 3$, and then we can get the relations via Eq. (4) + Eq. (5) − Eq. (6) with the texture variable eliminated:

$$\frac{1}{L-1} + \frac{1}{L-2} = (\tilde{k}_{1,1}\{\boldsymbol{C}_1\} + \tilde{k}_{1,2}\{\boldsymbol{C}_2\} - \tilde{k}_{1,3}\{\boldsymbol{C}_3\}) - (\ln|\boldsymbol{\Sigma}_1| + \ln|\boldsymbol{\Sigma}_2| - \ln|\boldsymbol{\Sigma}_3|) = K.$$

Therefore the estimator of the second log-determinant moment is as follows:

$$\begin{cases} \hat{L}_{\mathrm{TLDM}} = \dfrac{3\hat{K} + 2 + \sqrt{\hat{K}^2 + 4}}{2\hat{K}}, \\ \hat{K} = (\langle \ln|\boldsymbol{C}_1|\rangle + \langle \ln|\boldsymbol{C}_2|\rangle - \langle \ln|\boldsymbol{C}_3|\rangle) - (\ln|\langle \boldsymbol{C}_1\rangle| + \ln|\langle \boldsymbol{C}_2\rangle| - \ln|\langle \boldsymbol{C}_3\rangle|). \end{cases} \tag{9}$$

The solutions of this estimator are obtained from a quadratic equation, and we accept the bigger one which is bigger than 2, satisfying the requirements of the Wishart distribution that $\hat{L}_{\mathrm{TLDM}} \geqslant d$. And the estimator does not have an ambiguous solution.

2.3 Fourth log-determinant moment-based estimator (FLDM)

Here we give the simpler estimator which gives the estimated value with a direct analytical expression.

From Eq. (5) − Eq. (4), we get

$$\tilde{k}_{1,2}\{\boldsymbol{C}_2\} - \tilde{k}_{1,1}\{\boldsymbol{C}_1\} = \psi^{(0)}(L-1) + \ln|\boldsymbol{\Sigma}_2| - \ln|\boldsymbol{\Sigma}_1| - (\ln L - \tilde{k}_1\{T\}). \tag{10}$$

From Eq. (6) − Eq. (5), we get

$$\tilde{k}_{1,3}\{\boldsymbol{C}_3\} - \tilde{k}_{1,2}\{\boldsymbol{C}_2\} = \psi^{(0)}(L-2) + \ln|\boldsymbol{\Sigma}_3| - \ln|\boldsymbol{\Sigma}_2| - (\ln L - \tilde{k}_1\{T\}). \tag{11}$$

From Eq. (10) − Eq. (11), we get the direct relation of the number of looks:

$$2\tilde{k}_{1,2}\{\boldsymbol{C}_2\} - \tilde{k}_{1,1}\{\boldsymbol{C}_1\} - \tilde{k}_{1,3}\{\boldsymbol{C}_3\} = \frac{1}{L-2} + 2\ln|\boldsymbol{\Sigma}_2| - \ln|\boldsymbol{\Sigma}_1| - \ln|\boldsymbol{\Sigma}_3|.$$

We can get the third estimator:

$$\hat{L}_{\mathrm{FLDM}} = 2 + \frac{1}{(2\langle \ln|\boldsymbol{C}_2|\rangle - \langle \ln|\boldsymbol{C}_1|\rangle - \langle \ln|\boldsymbol{C}_3|\rangle) - (2\ln|\langle \boldsymbol{C}_2\rangle| - \ln|\langle \boldsymbol{C}_1\rangle| - \ln|\langle \boldsymbol{C}_3\rangle|)}. \tag{12}$$

The calculation is simpler and the computing time of the statistics of the determinant is the same as before. The above new estimators are all aimed to eliminate the texture variable and the estimated value of the determinant may generate external bias and variance. The motivation for different combinations of equations is to find the optimal one in these combinations. This will be performed in the following simulations. It should be clear how the sub-matrices are selected. For example, to select a 2×2 sub-matrix from the 3×3 full one there are three ways. In fact, when we choose two equations from (4), (5) and (6), we can get three combinations as $\mathrm{C}_3^2 = 3$. When we use all the equations of (4), (5) and (6), (4)+(5)−(6) is the basic combination, that is according to TLDM, and others are the linear combinations of the basic combination and the combinations of two equations mentioned above. Since the SLDM3 almost gives the best estimation in many combinations, including TLDM, after our study, and other combinations would supply no more information, we conclude that SLDM3 should be the optimal combination. Here we use the average value of the sub-matrix, and this processing will improve the estimation accuracy. We can also extend these estimators to the multi-texture case [15] (see Appendix).

Table 1 Invalid ratio of different estimators in a K-distribution case with α=8

Sample size	2	4	8	16	32	64	128	256	512
TLDM	0.0178	0.0004	0	0		0	0	0	0
SLDM	0.0231	0.0011	0	0		0	0	0	0
SLDM2	0.0192	0.0005	0	0		0	0	0	0
SLDM3	0.0182	0.0004	0	0		0	0	0	0
FLDM	0.0360	0.0012	0	0		0	0	0	0
FOL	0.3952	0.1310	0.0192	0.0005		0	0	0	0

3 Results

In this part, the performance of different estimators is presented via the simulated data in Subsection 3.1, including both a multi-texture case and a non-zero Wishart case. In Subsection 3.2, the results of the estimation are analyzed, and a novel distribution classification method is proposed by coloring the image via second and third order log-cumulants of covariance matrix (MLC), which is helpful to assess the estimation result. The computational complexity is presented in Subsection 3.3.

We used simulated data and real data to compare the following methods in both the Gaussian case and the product model case:

(1) Maximum likelihood (ML) estimator [1];

(2) FOL Estimator [12];

(3) Second log-determinant moment-based (SLDM, SLDM2, SLDM3) estimator;

(4) Third log-determinant moment-based (TLDM) estimator;

(5) Fourth log-determinant moment-based (FLDM) estimator.

The ML estimator is derived based on the log-determinant moment of the multilook polarimetric covariance matrix. The FOL estimator can be only used in the case of K-distribution. The new methods of (3)–(5) use the first order log-determinant cumulants which are adaptive to any product model. The results of simulation data and real data are presented in this section.

3.1 Synthetic data

The synthetic data for Wishart and non-Gaussian distributions with sample size $N = 1000000$ are used to compare the performance of the estimators. Firstly, the Wishart matrix samples are obtained from a homogeneous region in the NASA/JPL AIRSAR L-band image of Flevoland. Secondly, the scaled texture variable is generated to form the product model. The number of looks is $L = 10$. Here we assume the texture variable obeys gamma distribution or inverse gamma distribution (The product model corresponds to a K distribution or a G0 distribution). We find all the estimators except ML will generate invalid estimates for a small sample size. Table 1 shows that the SLDM3 and TLDM methods almost have the least invalid ratio. It should be noted that the invalid estimates have been deleted in the following evaluation.

In the following Figures 1–3, the simulation results are given for different sample sizes. The "UCRB" in Figures 1–3 is Cramer-Rao bound, which is calculated in the Wishart case [1]. The upper panel of Figure 1 displays the estimated bias versus sample size. The order of performance is the same with variance versus sample size, as shown in the middle panel. The lower panel displays the distribution of the ENL estimates when the sample size equals 512. The distribution was computed with a KDE estimator with an Epanechnikov kernel and the kernel bandwidth is h=0.1 [1]. The true number of looks is L=10.

Figure 1 shows the results of different estimators under K distribution simulated data. It can be seen that when the shape parameter is small, the SLDM3 and TLDM estimators rank first, followed by SLDM2, SLDM, FLDM, FOL and ML. When the shape parameter is moderate, the FOL estimator ranks first, followed by SLDM3, TLDM, SLDM2, SLDM, FLDM and ML.

From Figure 2, we can see for a general G0 distribution with a moderate shape parameter that the SLDM3 and TLDM rank first, followed by estimators SLDM2, SLDM, FLDM, FOL and ML. From

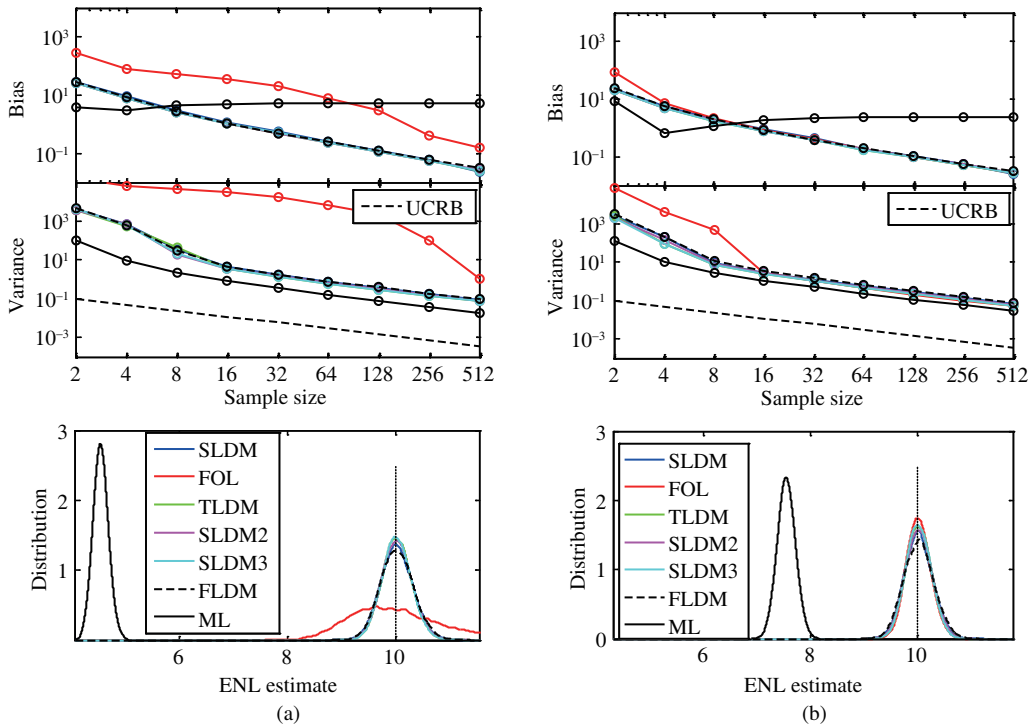

Figure 1 (Color online) The bias, variance and distribution estimates for the SLDM, TLDM, FLDM, FOL and ML estimators, calculated from general K-distribution data (The estimation performance can be ranked as FOL>SLDM3≈TLDM>SLDM2 >SLDM>FLDM>ML). (a) $\alpha = 2$; (b) $\alpha = 8$.

Figures 1 and 2, it can be seen that the SLDM3 and the TLDM are the best in all cases. And we can see that the bias of ML is not monotonic except in the Wishart case. It should be pointed out that when the sample size is small, the estimates are overestimated, and when the sample size is larger, they will be underestimated. The estimates itself is monotonic.

In fact, the assumption of a Wishart and product model with a fully correlated texture may not always be reasonable; sometimes the Gaussian scatter vector may be a non-zero mean [16], and the texture is not fully related in the different polarization channels [7]. We have done the simulation in both the non-zero Wishart case and the texture-non-correlated case in Figure 3, and the results show that the proposed methods still have good performance though it may be a little underestimate [see Appendix]. The bias is not monotonic (the ENL itself is monotonic), and we find when sample size is near 16–64 the estimate will get the least bias.

3.2 Real data

Now we use the real data to assess different estimators by using the same unsupervised estimation method as Anfinsen [1]. We chose two data sets from the PolSAR-Pro software received by the airborne L-band NASA/JPL AIRSAR instrument: one image of the San Francisco Bay area in California, USA, from 1988 with a pixel resolution of about 10 m×10 m, and the other image of an agricultural area in Flevoland, Netherlands, from 1989 with a pixel resolution of about 10 m×6.7 m supplied by ESAR/OP_ AIRFIELD. Both data sets are presented by four-looked coherency matrices.

(1) Unsupervised estimation

The traditional ENL is estimated by selecting a region of interest, while some research has been done to develop a fully automatic estimation algorithm avoiding manual selection of a region of interest [17–20]. Since all these methods are related to only one polarization at a time, Anfinsen proposed a new unsupervised estimator based upon the polarimetric ML estimator [1] which follows the approach of Ref. [18] and computes a single statistic of ENL, producing a one-dimensional distribution of small sample ENL estimates when the overall distribution of estimates is dominated by truly Wishart-distributed samples.

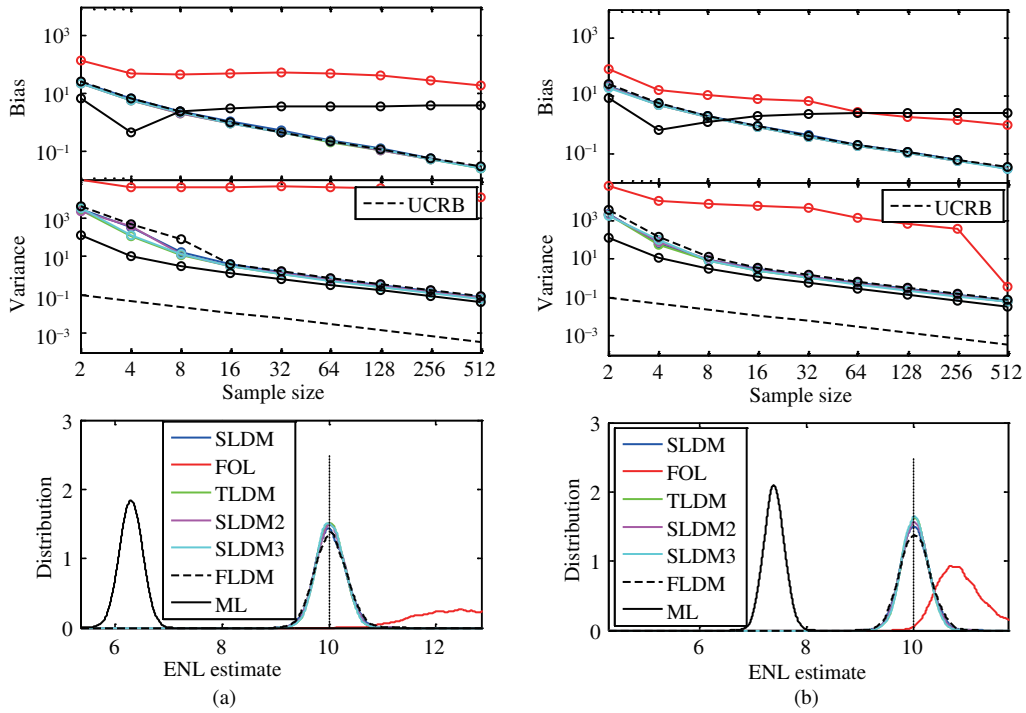

Figure 2 (Color online) The bias, variance and distribution estimates for the SLDM, TLDM, QLDM and QE estimators, calculated from general G0-distribution data (The estimation performance can be ranked as SLDM3≈TLDM>SLDM2>SLDM >FLDM>FOL>ML). (a) $\lambda = 5$; (b) $\lambda = 8$.

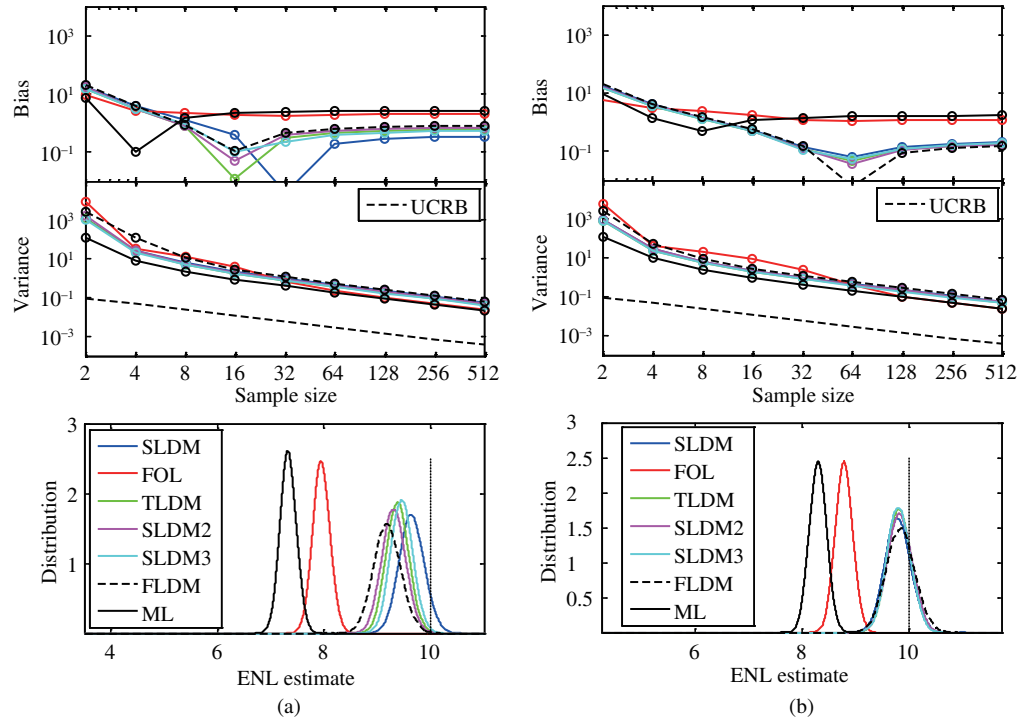

Figure 3 (Color online) ENL estimation results calculated from simulated data with (a) non-zero-mean Wishart model and (b) texture-non-correlated product model, respectively.

Figure 4 shows the results of our new estimators for different window sizes. Each image computes the estimators in a sliding window of size $k \times k$ pixels, through the whole image. The window size was changed

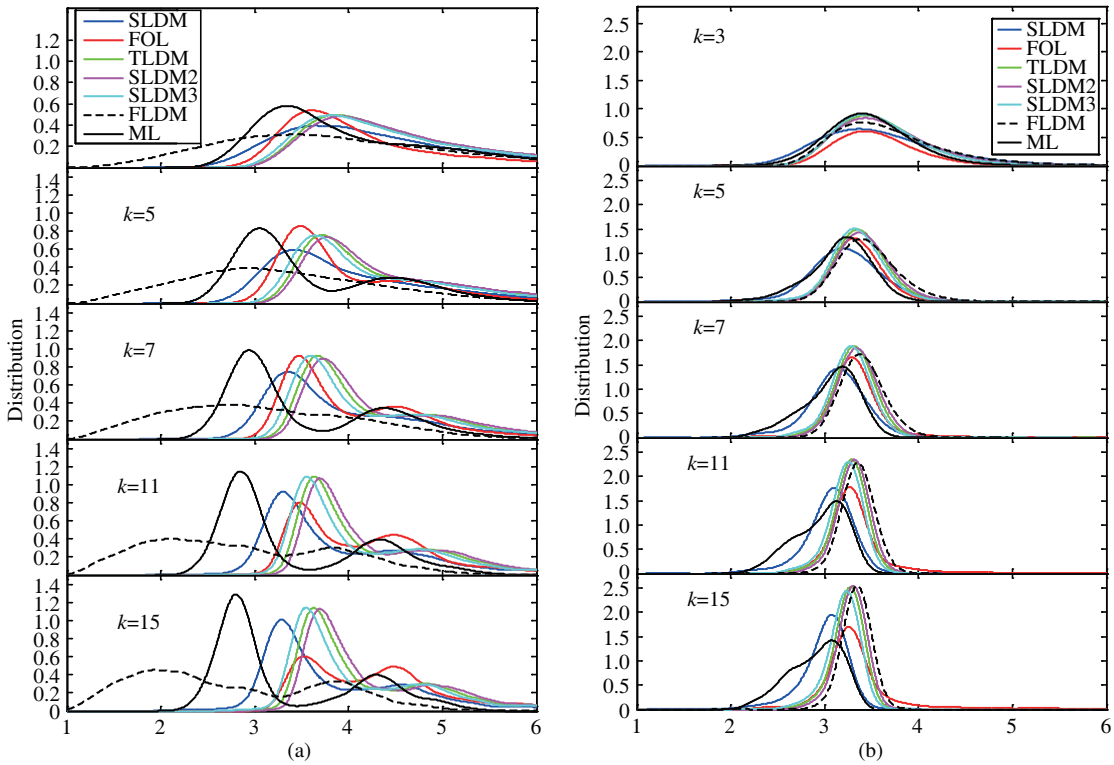

Figure 4 (Color online) Distribution estimates for all estimators calculated from the AIRSAR image of (a) San Francisco and (b) Flevoland. ENL estimated with window sizes of $k\{3, 5, 7, 11, 15\}$.

from k=3 to k=15. We used a KDE with an Epanechnikov kernel function and a kernel bandwidth of h=0.1 [1].

To decide the distribution type of different areas, Anfinsen presented a new goodness-of-fit (GOF) method based on log-cumulants of covariance matrix (MLC) [21]. It shows that we can use the MLC to study the Wishart-dominated hypothesis of the image. We plot the MLC diagram and then color it. It can be imagined that each point on the MLC diagram presents a type of distribution with specific parameters.

Figure 5 shows the segmented MLC diagram and the segmented MLC image of San Francisco. Figure 5(a) is the segmented MLC diagram. We can see that the Wishart point corresponding to {k3,k2} equals {0,0}, which means that we have canceled the effect of the number of looks. Each point on the diagram is a relative value by canceling the effect of the number of looks. When the window size is k=5, Figures 5(b) and (c) give the estimates of ML and SLDM3. It is easy to see that the ML method underestimates across a large area and SLDM3 gives the best results. Figure 5(d) gives the MLC image of San Francisco after the ENL has been canceled, and the value of ENL is estimated by SLDM3. From Figure 5(d) we can see that only the ocean and vegetable areas are distributed close to a Wishart model, while the large land area distribution is far from the Wishart model, and may be that of the product model. Therefore, we can see that the unsupervised estimation by Anfinsen does not work perfectly here as too many underestimates dominate the estimation result. As Anfinsen says, the ocean area will generate an overestimation of its scattering characteristics [1], so the vegetable area was chosen to estimate the global ENL shown in Table 2 using supervised method. It can also be seen that if we were to use the product model in some special area of the real image, it is better to estimate the ENL from the local area, though it may not be the global one.

Figure 6 gives the ENL estimates and the MLC image of Flevoland after the cancelation of ENL when the window size is k=5. We can see ML still gets underestimates, and most areas except the river are near to a Wishart distribution. That is to say the distribution is dominated by Wishart-distributed samples and the ML method is suitable for this case. We can see that the estimated results of the SLDM3 method

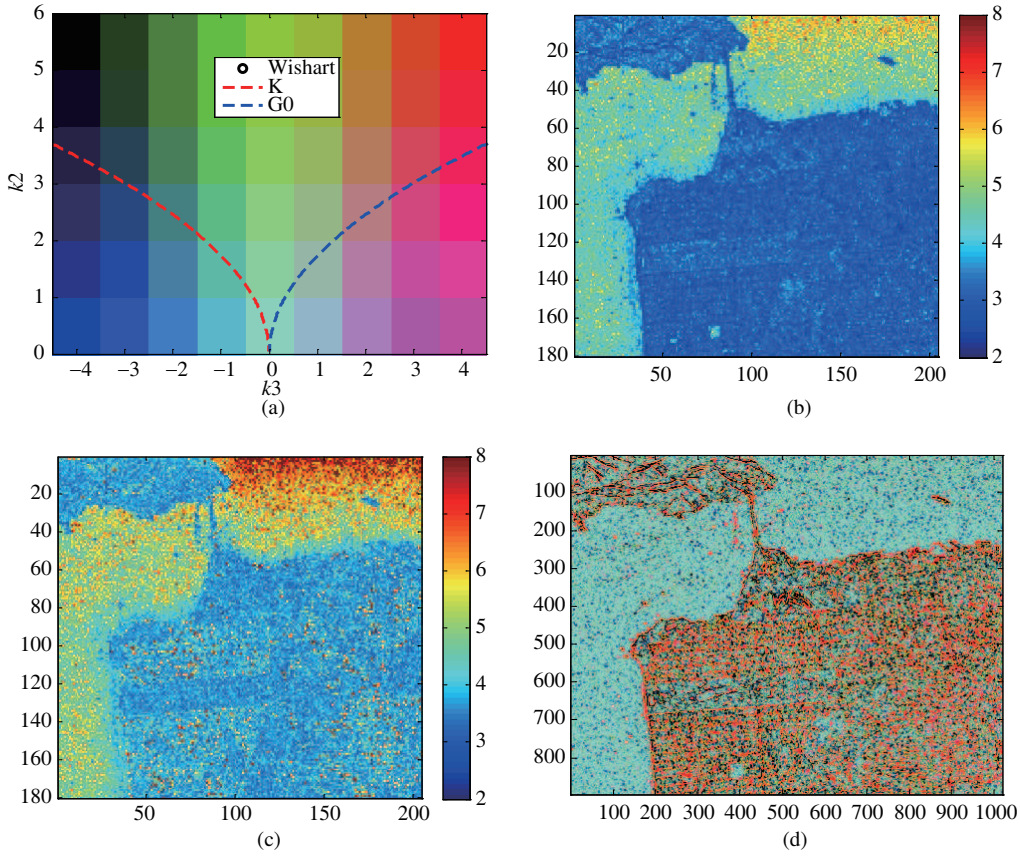

Figure 5 (Color online) (a) The segmented MLC diagram; (b) estimates image of ML; (c) estimates image of SLDM3; (d) the segmented MLC image of San Francisco.

Table 2 The estimation result of the ENL of San Francisco when k=5, k=7 and k=11

San Francisco	ML (Vegetable)	ML	SLDM	SLDM2	SLDM3	TLDM	FLDM	FOL
ENL (k=5)	3.579	3.057	3.426	3.776	3.644	3.724	2.929	3.493
ENL (k=7)	3.563	2.941	3.362	3.731	3.597	3.671	2.733	3.476
ENL (k=11)	3.523	2.848	3.308	3.695	3.557	3.638	2.122	3.485

Table 3 The estimation result of the ENL of Flevoland when k=5 , k=7 and k =11

Flevoland	ML (Vegetable)	ML	SLDM	SLDM2	SLDM3	TLDM	FLDM	FOL
ENL (k=5)	3.365	3.246	3.198	3.372	3.320	3.358	3.394	3.317
ENL (k=7)	3.347	3.196	3.149	3.342	3.285	3.317	3.375	3.291
ENL (k=11)	3.316	3.130	3.103	3.319	3.254	3.292	3.356	3.268

are similar in different windows in both images, while many invalid estimates occur in the ocean area for the FOL estimator, and the ML estimator gives many underestimates.

Tables 2 and 3 give the estimation results for the San Francisco and Flevoland images when the window size is k=5, k=7 and k=11. We use the supervised estimation to assess the estimation of ENL, by choosing the homogeneous region (the vegetable area). We can calculate the ENL with the ML method from the vegetable area in San Francisco Bay, whose value is derived as 3.523 in Table 2 and the estimated ENL is 3.316 in Table 3 in the Flevoland image when the window size is 11. In Table 2, it can be seen that the ML method gives a result of 3.057, which is near the precious estimation by Anfinsen when the window size is k=5 without bias correction [1], and this happens just because non-Wishart distributions dominate the image, which should be underestimated. From Figure 5 we can see that the values of ENL in different areas are quite different. The global ENL is estimated as an average value. As an average value of the

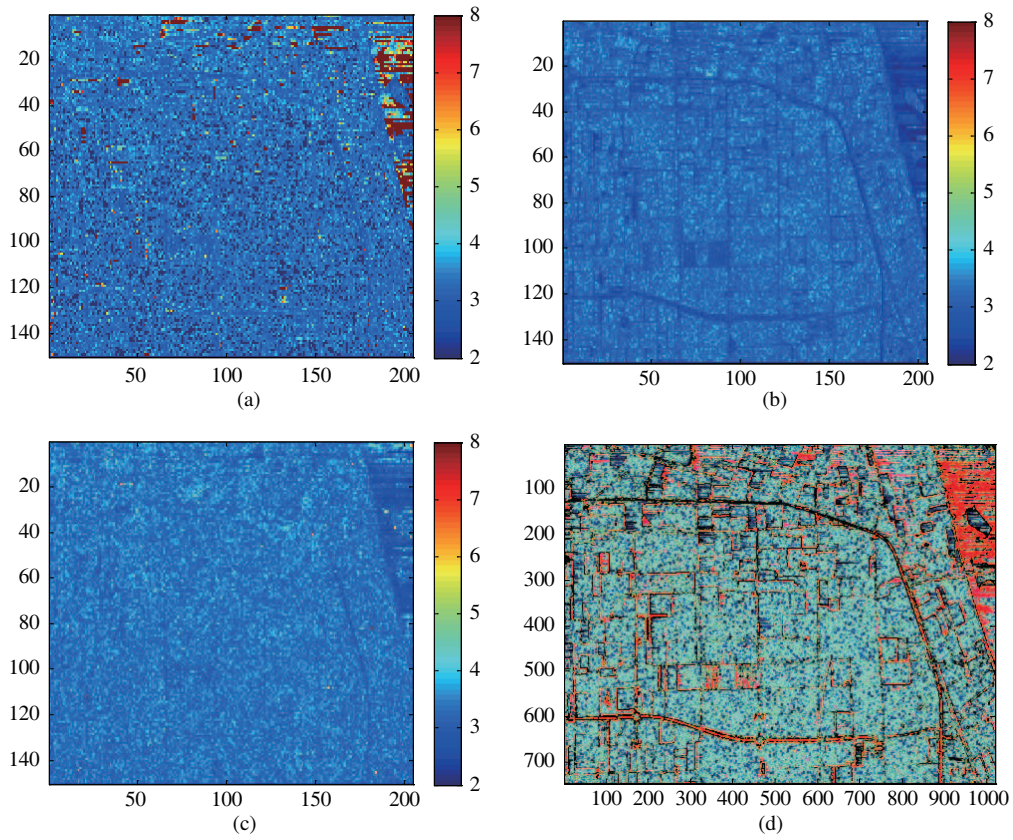

Figure 6 (Color online) The ENL estimates and the colored MLC image of San Francisco when the window size is 5. (a) Estimates of FOL; (b) estimates of ML; (c) estimates of SLDM3; (d) MLC image of Flevoland (SLDM3).

global ENL, SLDM3 gives a more acceptable estimate as 3.557. In the Flevoland image most areas are distributed as a Wishart distribution, and therefore all the estimators appear to have little difference. When the window size is 5, Anfinsen gives the estimate as 3.246 by the ML method. By choosing the vegetable area, we get the supervised estimate as 3.316 when the window size is k=11. We can see that when the window size is k=5, SLDM3 gives the estimate as 3.320, which is the best estimate among all the estimators.

(2) Effect of window size

From Figure 7, we can study the accuracy of ENL estimates using simulated data and real data when the window size increases. We can see the modes become narrower and the variance becomes lower. But the probability of mixed classes within the estimation window increases, which may generate underestimates. According to the following simulation results, it seems reasonable to use the 5×5 window size, with which it is possible to degrade the mixed class effect, while keeping a low variance and bias to obtain the required accuracy. It can be seen that the ML-ML estimator gives a good performance in a small window size or for a few samples in the Wishart assumption, while it is not suitable for a texture model. It can also be seen that if the homogeneous area, where the speckle is fully developed as a Wishart distribution, is large in real datasets, the ML-ML estimator may be a good estimator, especially in the case of few samples with the smallest window size. As is also shown in the Flevoland image, the estimated ENL by the ML-ML method is 3.38 when the windows size is 2, which is near the global ENL of 3.32 (Table 3).

3.3 Computational complexity

The computational complexity of the different methods is presented in this part. The performance measure is central processing unit (CPU) time, which is measured by the Matlab profile function, on a

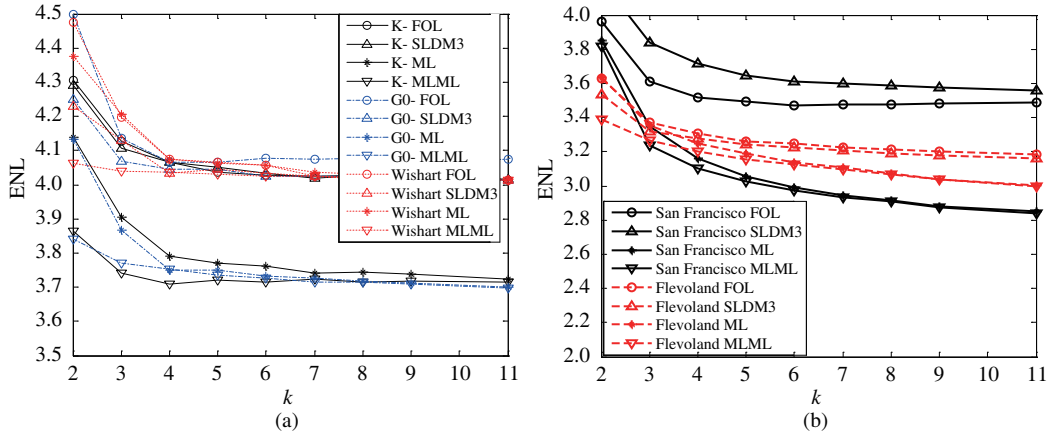

Figure 7 (Color online) The estimates of ENL as function of window size for different estimators. Effect of window size (a) simulated data and (b) real data.

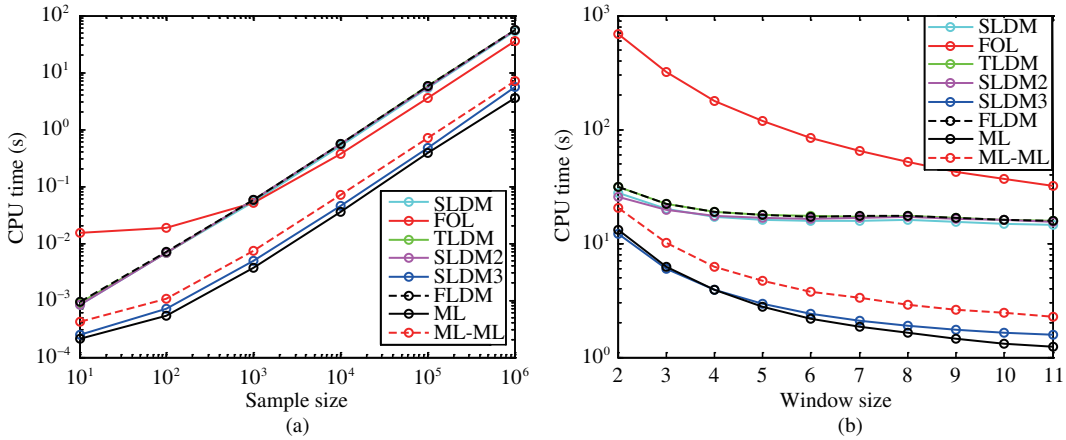

Figure 8 (Color online) Computational Complexity of all estimators measured in CPU time per estimate calculation as function of (a) sample size and (b) window size.

3.1 GHz Intel Core i5 processor. Figure 8(a) displays the CPU time required per estimate calculation as a function of sample size. Figure 8(b) displays the CPU time required per estimation calculation as a function of window size when the number of all samples is constant.

The figure shows the ML estimator has the lowest computational cost, followed by the SLDM3. The other estimators, such as SLDM, SLDM2, TLDM, FLDM, and FOL, have a similar computational cost. The ML-ML estimator has almost twice the ML's cost. If the window size becomes larger, the computational cost becomes lower. Therefore, the SLDM3 estimator is the recommended one because of its high accuracy and low computational cost.

4 Conclusion

It motivates us to find a method to eliminate the effect of texture that the existing ENL estimators are not suitable for the product model case. We found the sub-matrix, including the texture variable, can be used to eliminate the same variable in the full covariance matrix. These analytic estimators use different orders of covariance matrices, and utilize more of the available statistical information. To assess the results of the different estimators in different environments, we present a novel distribution classification method by coloring the image via second- and third-order MLC. The results are verified by the experiments using both simulated data and real data. We find the second log-determinant moment estimator (SLDM3) is the best estimator of the novel estimators, both in the Gaussian case and the product model case,

with much higher accuracy and less computational complexity, and is the recommended estimation under general conditions.

Acknowledgements The work was supported by National Natural Science Foundation of China (Grant No. 61372165).

Conflict of interest The authors declare that they have no conflict of interest.

References

1 Anfinsen S N, Doulgeris A P, Eltoft T. Estimation of the equivalent number of looks in polarimetric synthetic aperture radar imagery. IEEE Trans Geosci Remote Sens, 2009, 47: 3795–3809
2 Oliver C, Quegan S. Understanding Synthetic Aperture Radar Images. 2nd ed. Raleigh: Sci Tech Publishing, 2004
3 Cumming I G, Wong F H. Digital Processing of Synthetic Aperture Radar Data: Algorithms and Implementation. Norwood: Artech House, 2005
4 Lee J-S, Grunes M R, Kwok R. Classification of multilook polarimetric SAR imagery based on complex Wishart distribution. Int J Remote Sens, 1994, 15: 229–231
5 Lee J-S, Grunes M R, Ainsworth T L, et al. Unsupervised classification using polarimetric decomposition and the complex Wishart distribution. IEEE Trans Geosci Remote Sens, 1999, 37: 2249–2259
6 Kersten P R, Lee J-S, Ainsworth T L. Unsupervised classification of polarimetric synthetic aperture radar images using fuzzy clustering and EM clustering. IEEE Trans Geosci Remote Sens, 2005, 43: 519–527
7 Frery A C, Correia A H, Freitas C C. Classifying multifrequency fully polarimetric imagery with multiple sources of statistical evidence and contextual information. IEEE Trans Geosci Remote Sens, 2007, 45: 3098–3109
8 Doulgeris A P, Anfinsen S N, Eltoft T. Classification with a non-Gaussian model for PolSAR data. IEEE Trans Geosci Remote Sens, 2008, 46: 2999–3009
9 Conradsen K, Nielsen A A, Schou J, et al. A test statistic in the complex Wishart distribution and its application to change detection in polarimetric SAR data. IEEE Trans Geosci Remote Sens, 2003, 41: 4–19
10 Lee J-S, Schuler D L, Lang R H, et al. K-distribution for multi-look processed polarimetric SAR imagery. In: Proceedings of the IEEE International Geoscience Remote Sensing Symposium (IGARSS'94), Pasadena, 1994, 4: 2179–2181
11 Liu T, Cui H G, Xi Z M X, et al. Texture-invariant estimation of equivalent number of looks based on trace moments in polarimetric radar imagery. IEEE Geosci Remote Sens Lett, 2014, 11: 1129–1133
12 Doulgeris A P, Anfinsen S N, Eltoft T. Automated non-Gaussian clustering of polarimetric synthetic aperture radar images. IEEE Trans Geosci Remote Sens, 2011, 49: 3665–3676
13 Liu T, Cui H G, Gao J. Statistics of the determinant of the Wishart distributed matrix and its application to parameter estimation. Acta Electron Sinica, 2013, 41: 1231–1237
14 Anfinsen S N, Eltoft T. Application of the matrix-variate Mellin transform to analysis of polarimetric radar images. IEEE Trans Geosci Remote Sens, 2011, 49: 2281–2295
15 Eltoft T, Anfinsen S N, Doulgeris A P. A multitexture model for multilook polarimetric synthetic aperture radar data. IEEE Trans Geosci Remote Sens, 2013, 52: 2910–2919
16 Maaref A, Aissa S. Joint and marginal eigenvalue distribution of (non)central complex Wishart matrices and PDF-based approach for characterizing the capacity statistics of MIMO Ricean and Rayleigh fading channels. IEEE Trans Wirel Commun, 2007, 6: 3607–3619
17 Lee J-S, Hoppel K, Mango S A. Unsupervised estimation of speckle noise in radar images. Int J Imaging Syst Tech, 1992, 4: 298–305
18 Foucher S, Boucher J M, Benie G B. Maximum likelihood estimation of the number of looks in SAR images. In: Proceedings of the International Conference of Microwave, Radar and Wireless Communications, Wroclaw, 2000, 2: 657–660
19 Cui Y, Zhou G, Yang J, et al. Unsupervised estimation of the equivalent number of looks in SAR images. IEEE Geosci Remote Sens Letts, 2011, 8: 710–714
20 Xu B, Cui Y, Zhou G, et al. Unsupervised speckle level estimation of SAR images using texture analysis and AR model. IEICE Trans Commun, 2014, 97: 691–698
21 Anfinsen S N, Doulgeris A D, Eltoft T. Goodness-of-fit tests for multilook polarimetric radar data based on the Mellin transform. IEEE Trans Geosci Remote Sens, 2011, 49: 2281–2295

Appendix A

In Ref. [15] we can see the log-cumulants of the multi-texture models can be summarized as

$$k_v\{\boldsymbol{T}\} = \begin{cases} d^v k_v\{T\} : \text{scalar} - \text{texture}, \\ d_{co}^v k_v\{T_{co}\} + d_x^v k_v\{T_x\} : \text{dual} - \text{texture}, \\ \sum\limits_{i=1}^{d} k_v\{T_i\} : \text{three} - \text{texture}. \end{cases} \tag{A1}$$

The scalar texture case corresponds to the familiar scalar product model, where the texture variables are identical for all polarizations. This case is discussed in detail in our paper. Here we emphasize the analyses of other cases.

For the three-texture cases:

If $d = 1$, we get

$$\tilde{k}_{1,1}\{\boldsymbol{C}_{1-1}\} = \psi^{(0)}(L) + \ln|\boldsymbol{\Sigma}_{1-1}| - \ln L + \tilde{k}_1\{T_1\}, \tag{A2.1}$$

$$\tilde{k}_{1,1}\{\boldsymbol{C}_{1-2}\} = \psi^{(0)}(L) + \ln|\boldsymbol{\Sigma}_{1-2}| - \ln L + \tilde{k}_1\{T_2\}, \tag{A2.2}$$

$$\tilde{k}_{1,1}\{\boldsymbol{C}_{1-3}\} = \psi^{(0)}(L) + \ln|\boldsymbol{\Sigma}_{1-3}| - \ln L + \tilde{k}_1\{T_3\}. \tag{A2.3}$$

With Eq. (A2.1) + Eq. (A2.2) + Eq. (A2.3), we get

$$\tilde{k}_{1,1}\{\boldsymbol{C}_1\} = \psi^{(0)}(L) + \ln|\boldsymbol{\Sigma}_1| - \ln L + \tilde{k}_1\{\boldsymbol{T}\}, \tag{A2.4}$$

where $\tilde{k}_{1,1}\{\boldsymbol{C}_1\} = (\tilde{k}_{1,1}\{\boldsymbol{C}_{1-1}\}+\tilde{k}_{1,1}\{\boldsymbol{C}_{1-1}\}+\tilde{k}_{1,1}\{\boldsymbol{C}_{1-1}\})/3$, $\ln|\boldsymbol{\Sigma}_1|=(\ln|\boldsymbol{\Sigma}_{1-1}|+\ln|\boldsymbol{\Sigma}_{1-2}|+\ln|\boldsymbol{\Sigma}_{1-3}|)/3$ and $\tilde{k}_1\{\boldsymbol{T}\} = (\tilde{k}_1\{T_1\} + \tilde{k}_1\{T_2\} + \tilde{k}_1\{T_3\})/3$, which has the same formation as Eq. (4).

If $d = 2$, we get

$$\tilde{k}_{1,2}\{\boldsymbol{C}_{2-12}\} = \psi^{(0)}(L) + \psi^{(0)}(L-1) + \ln|\boldsymbol{\Sigma}_{2-12}| - 2\ln L + (\tilde{k}_1\{T_1\} + \tilde{k}_1\{T_2\}), \tag{A3.1}$$

$$\tilde{k}_{1,2}\{\boldsymbol{C}_{2-13}\} = \psi^{(0)}(L) + \psi^{(0)}(L-1) + \ln|\boldsymbol{\Sigma}_{2-13}| - 2\ln L + (\tilde{k}_1\{T_1\} + \tilde{k}_1\{T_3\}), \tag{A3.2}$$

$$\tilde{k}_{1,2}\{\boldsymbol{C}_{2-23}\} = \psi^{(0)}(L) + \psi^{(0)}(L-1) + \ln|\boldsymbol{\Sigma}_{2-23}| - 2\ln L + (\tilde{k}_1\{T_2\} + \tilde{k}_1\{T_3\}), \tag{A3.3}$$

With Eq. (A3.1) + Eq. (A3.2) + Eq. (A3.3), we get

$$\tilde{k}_{1,2}\{\boldsymbol{C}_2\} = \psi^{(0)}(L) + \psi^{(0)}(L-1) + \ln|\boldsymbol{\Sigma}_2| - 2\ln L + 2\tilde{k}_1\{\boldsymbol{T}\}, \tag{A3.4}$$

where $\tilde{k}_{1,2}\{\boldsymbol{C}_2\} = (\tilde{k}_{1,2}\{\boldsymbol{C}_{2-12}\} + \tilde{k}_{1,2}\{\boldsymbol{C}_{2-13}\} + \tilde{k}_{1,2}\{\boldsymbol{C}_{2-23}\})/3$, $\ln|\boldsymbol{\Sigma}_2| = (\ln|\boldsymbol{\Sigma}_{2-12}| + \ln|\boldsymbol{\Sigma}_{2-13}| + \ln|\boldsymbol{\Sigma}_{2-23}|)/3$, which has the same formation as Eq. (5).

If $d = 3$, we get

$$\tilde{k}_{1,3}\{\boldsymbol{C}_3\} = \psi^{(0)}(L) + \psi^{(0)}(L-1) + \psi^{(0)}(L-2) + \ln|\boldsymbol{\Sigma}_3| - 3\ln L + 3\tilde{k}_1\{\boldsymbol{T}\}, \tag{A4}$$

which has the same formation as Eq. (6).

With Eq. (A2.4)×2− Eq. (A3.4), using Eq. (3), we get

$$L = 1 + \frac{1}{(2\tilde{k}_{1,1}\{\boldsymbol{C}_1\} - \tilde{k}_{1,2}\{\boldsymbol{C}_2\}) - (2\ln|\boldsymbol{\Sigma}_1| - \ln|\boldsymbol{\Sigma}_2|)}, \tag{A5}$$

which has the same formation as Eq. (7). And we can easily obtain the novel estimator expressions for multi-texture cases, which have the same expressions as a scalar case.

For dual-texture, following the same steps, we can get the same estimator expressions as a scalar case.